Dynamics and coherence resonance in a thermosensitive neuron driven by photocurrent*

Ying Xu(徐莹)[1,2], Minghua Liu(刘明华)[3,1], Zhigang Zhu(朱志刚)[1], and Jun Ma(马军)[1,4,†]

[1] *Department of Physics, Lanzhou University of Technology, Lanzhou* 730050, *China*
[2] *Department of Physics, Central China Normal University, Wuhan* 430079, *China*
[3] *Electrical Engineering College, Northwest Minzu University, Lanzhou* 730124, *China*
[4] *School of Science, Chongqing University of Posts and Telecommunications, Chongqing* 430065, *China*

(Received 16 May 2020; revised manuscript received 8 June 2020; accepted manuscript online 18 June 2020)

A feasible neuron model can be effective to estimate the mode transition in neural activities in a complex electromagnetic environment. When neurons are exposed to electromagnetic field, the continuous magnetization and polarization can generate nonlinear effect on the exchange and propagation of ions in the cell, and then the firing patterns can be regulated completely. The conductivity of ion channels can be affected by the temperature and the channel current is adjusted for regulating the excitability of neurons. In this paper, a phototube and a thermistor are used to the functions of neural circuit. The phototube is used to capture external illumination for energy injection, and a continuous signal source is obtained. The thermistor is used to percept the changes of temperature, and the channel current is changed to adjust the excitability of neuron. This functional neural circuit can encode the external heat (temperature) and illumination excitation, and the dynamics of neural activities is investigated in detail. The photocurrent generated in the phototube can be used as a signal source for the neural circuit, and the thermistor is used to estimate the conduction dependence on the temperature for neurons under heat effect. Bifurcation analysis and Hamilton energy are calculated to explore the mode selection. It is found that complete dynamical properties of biological neurons can be reproduced in spiking, bursting, and chaotic firing when the phototube is activated as voltage source. The functional neural circuit mainly presents spiking states when the photocurrent is handled as a stable current source. Gaussian white noise is imposed to detect the occurrence of coherence resonance. This neural circuit can provide possible guidance for investigating dynamics of neural networks and potential application in designing sensitive sensors.

Keywords: thermosensitive neuron, thermistor, phototube, bifurcation, coherence resonance

PACS: 87.19.lq, 87.18.Hf, 05.45.−a **DOI:** 10.1088/1674-1056/ab9dee

1. Introduction

Nervous system can encode and propagate physiological electrical signals from several routes synchronously, and it is considered as an effective intelligent signal processing system because of the multiple biological function in neurons. The occurrence of electrophysiological activities, e.g., random ions diffusion in the cell and pumping of ions (calcium, potassium) across the membrane channels, can break the balance of intracellular and extracellular ions concentrations, as a result, firing can be induced to trigger action potentials and pulses. Started from the pioneering work finished by Hodgkin-Huxley,[1] many artificial neurons and neuron models[2–6] have been proposed to calculate the dynamics in neural activities by applying external stimulus and parameter exciting.[7–10] In addition, the biophysical function of astrocyte[11–13] has been confirmed to adjust the release and exchange of calcium, in which the membrane potential of cell can be adjusted effectively. Therefore, neuron-coupled astrocyte networks[14–16] are used to estimate the mode selection and transition in neurons. From the viewpoint of cell development and genetics, the formation of synaptic structure accounts for the functional requirements of biological neurons, in which the activation and release of neural activities are dependent on the external stimuli. For example, formation of autapse[17,18] can enhance the self-adaption of neuron to external stimuli, and an auxiliary feedback loop[19] is formed to correct the blocked signal propagation along the injured axon. Local distribution of autapse in networks can induce continuous pulses and wave fronts for regulating the spatial behaviors,[20–23] and the activation of autapse in an isolated neuron[24–27] can enable appropriate mode selection in the electrical activities. For a complete review on collective behaviors of neural networks and physical mechanism in neurodynamics, readers can find possible suggestions about model setting, pattern formation, and synchronization stability in neuron and neural networks.[28–30]

As is well known, the dynamics of network is dependent on the local kinetics of node and connection topology between nodes. In a practical way, the biophysical effect and property should be considered for building more reliable neuron models or artificial neurons with high intelligence. As suggested in Ref. [31], magnetic flux can be introduced

*Project supported by the National Natural Science Foundation of China (Grant No. 11672122).
†Corresponding author. E-mail: hyperchaos@lut.edu.cn; hyperchaos@163.com

to estimate the effect of electromagnetic induction in neuron by incorporating the physical property of magnetic-flux controlled memristor.[32–35] In fact, the involvement of memristor to couple neurons can form memristive synapse[36–38] and then the synaptic plasticity can be released by applying time-varying radiation and electric stimuli on the neurons and neural networks.[39–42] Furthermore, it is confirmed that field coupling[43–46] provides another effective way to stabilize neurons in network even synapse coupling is suppressed completely. Both of capacitor and inductor are important electronic components for building and connecting nonlinear circuits, and time-varying field can be induced in these components[47] to capture and pump field energy across the coupling channels. In particular, the electric field coupling via capacitor connection explains the physical mechanism for differential coupling[48,49] while the magnetic field coupling via induction coil provides new definition for integral coupling[50–52] between nonlinear circuits. When memristor is used to couple nonlinear circuits,[53–55] synchronization can be obtained by applying appropriate values for the intrinsic parameters in the coupling channel, in which field energy is pumped and exchanged effectively. In addition, Josephson junction can also be used to couple neural circuits, and synchronization is realized by taming the channel current and phase error for the junction.[56] In a word, these functional components can be used to build functional circuits,[57–60] and they are effective to pump field energy across the coupling channels and the combination of these components can design hybrid synapse for neural circuits. Phototube is an important physical component and the external optical signal can be captured for generating photocurrent, which is effective to excite neurons. Therefore, phototube can be used as signal source (voltage source or current source) for activating neural circuits and the light-dependent neural circuit[61] can show potential application in designing artificial electronic eyes. Temperature has distinct impact on neural activities because the excitability of neuron and conduction of channels can be changed.[62–65] Thermistor is also an important electronic component, and its resistance can be adjusted by the temperature. Therefore, the nonlinear circuit can be used as artificial sensor for detecting the changes of temperature when a thermistor is coupled with the neural circuit.

Biological neurons can trigger different kinds firing patterns in the electronical activities. Surely, mathematical neuron models can be proposed to reproduce the main dynamical properties of realistic neurons when the variables can present a variety of oscillation modes. Furthermore, the intrinsic parameters and external equivalent forcing current can be changed to get different firing patterns. However, the most important thing is to know the biophysical mechanism for encoding external signals and obtain artificial signal processor and sensor guided by the self-adaption function of biological neurons. It is interesting to design artificial neurons with more biophysical functions. For example, the eyes can percept external illumination and appropriate visual signal is induced to propagate along the loop of the visual nervous system. That is, external optical signal is converted into equivalent current to excite the nervous system and right gaits can be activated. The skin can percept the heat effect when the ambient temperature is changed, and the activation of cells induced by temperature can also be effective to regulate the channel current of cells. Phototube can capture external illumination and then covert the light with high frequency into photocurrent. Therefore, it can be used as signal source to drive nonlinear circuits. Thermistor can change the resistance when the temperature is changed, and the branch current can be adjusted when a thermistor is connected to the circuit. Both thermistor and phototube can be used as sensitive sensors. The function of nonlinear circuit can be enhanced when thermistor and phototube are included to build a neural circuit by taming the intrinsic parameters, external temperature for thermistor and illumination for phototube. In this way, this neural circuit and neuron become dependent on the temperature and external radiation. In this paper, both of thermistor and phototube are used to rebuild a functional neural circuit. The phototube is used as signal source for activating the circuit and thermistor in the branch is used to percept the temperature effect. The circuit is built and dynamics in this neural circuit is discussed in detail for providing guidance and potential application in intelligent computing and artificial neural networks.

In Section 2, the functional neural circuit is built by incorporating a thermistor and a phototube, and scale transformation is applied to obtain a neuron model, which can encoding light (illumination) and temperature (heat). In Section 3, numerical results are presented by calculating the bifurcation analysis and statistical coherence, and appropriate discussion is supplied to explain the biophysical mechanism of this functional neuron. In the last section, conclusion is presented.

2. Model and scheme

Biological neurons can be thought as intelligent and smart signal processors and thus functional artificial circuits can be designed to realize these functions. In generic way, most of these nonlinear circuits can be tamed in parameters and applying appropriate stimulus, and a neural circuit is obtained when the output voltage can produce similar firing patterns (quiescent, spiking, bursting, and chaotic states) as electronical activities from biological neurons. For simplicity, a capacitor is used to generate output voltage, an induction coil is used for generating time-varying current in the branch circuit, and a nonlinear resistor is used to induce nonlinear relation between voltage and current. When more physical components

are included, the function of the circuit can be enhanced. As reported in Refs. [66,67], a nonlinear circuit can be tamed to give similar behaviors generated in most of the biological neurons. For simplicity, a phototube is used as exciting source and a thermistor is used to replace the linear resistor in the simple oscillator circuit in Ref. [67]. The phototube is activated when external illumination is applied to generate continuous photocurrent for exciting the neural circuit, and the external temperature is changed to adjust the resistance of the thermistor for triggering time-varying branch/channel current. The circuit is presented in Fig. 1.

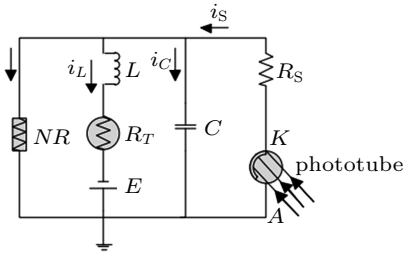

Fig. 1. Schematic diagram for the neural circuit, which is dependent on the illumination and temperature. NR is a nonlinear resistor, C is the capacitor, L represents an induction coil, R_T denote a thermistor, R and R_S are linear resistors, and E is a constant voltage source. K denotes the cathode and A represents the anode in the phototube. The relation between the resistance of thermistor and temperature T is estimated with $R_T = R_\infty \exp(B/T)$, and the material parameter B is determined by the activation energy q and the Boltzmann's constant K' with the dependence as $B = q/K'$.

The relation between the voltage and current of nonlinear resistor NR is estimated by

$$i_{NR} = -\frac{1}{\rho}\left(V - \frac{1}{3}\frac{V^3}{V_0^2}\right), \tag{1}$$

where ρ is the normalized parameter for resistance, V_0 represents the cutoff voltage, and V is the voltage across the nonlinear resistor. The photocurrent across the phototube is dependent on the external illumination and the material property of the cathode, and it can reach a saturation value when the intensity of external illumination is increased greatly. The relation between the photocurrent and voltage[61] across the phototube is estimated by

$$i_S = \frac{2I_H}{\pi}\arctan(V_S - V_a), \tag{2}$$

where V_a denotes the reverse cut-off voltage, V_S and I_H describe the voltage and saturation current across the phototube, respectively. According to the physical Kirchhoff's theorem, the circuit equations for Fig. 1 can be obtained by

$$\begin{cases} C\dfrac{\mathrm{d}V}{\mathrm{d}t} = i_S - i_L - i_{NR}, \\ L\dfrac{\mathrm{d}i_L}{\mathrm{d}t} = V - R_T i_L + E, \end{cases} \tag{3}$$

where V and i_L denote the output voltage across the capacitor C and the induction current across the induction coil L, respectively. The parameters R_T, C, L, E indicate the resistance of thermistor, capacitance, inductance, and constant voltage, respectively. In addition, the photocurrent across the phototube in the neural circuit can be approached by finding the solution in the following equation:

$$i_S = \frac{2I_H}{\pi}\arctan(V_S - V_a) = \frac{V_S - V}{R_S}, \tag{4}$$

where the variable V has the same expression used for describing the output voltage of the capacitor, V_S is the output voltage across the phototube, and R_S is the resistance of the linear resistor. In fact, the selection of resistor R_S dictates the output property of the signal source (exciting source). For example, the phototube can be handled as a voltage source when the resistor R_S is selected with a large resistance and then the voltage V_S can be varied in a large scope. On the other hand, the phototube can be treated as a current source by generating photocurrent with saturation value when the resistor R_S is fixed at small values. By applying standard scale transformation, these physical variables and parameters in the circuit equations can be replaced by

$$\begin{cases} x = \dfrac{V}{V_0}, \quad y = \dfrac{\rho i_L}{V_0}, \quad \tau = \dfrac{t}{\rho C}, \\ a = \dfrac{E}{V_0}, \quad b(T') = \dfrac{R_T}{\rho} = b_0 \exp\left(\dfrac{1}{T'}\right), \\ c = \dfrac{\rho^2 C}{L}, \quad \xi = \dfrac{\rho}{R_S}, \\ u_S = \dfrac{V_S \rho}{R_S V_0} = \xi\dfrac{V_S}{V_0}, \quad T' = \dfrac{T}{T_0} = \dfrac{T}{B}. \end{cases} \tag{5}$$

As a consequence, the circuit equations shown in Eq. (3) can be rewritten as

$$\begin{cases} \dfrac{\mathrm{d}x}{\mathrm{d}\tau} = x(1-\xi) - \dfrac{1}{3}x^3 - y + u_S, \\ \dfrac{\mathrm{d}y}{\mathrm{d}\tau} = c[x + a - b(T')y], \end{cases} \tag{6}$$

where the dimensionless variables x and y are mapped from the voltage and current, respectively. The variable x represents the membrane potential and y denotes the current across the membrane of the neuron. The neuron becomes dependent on the temperature and the external stimulus u_S can change the dynamics of the neuron. In fact, the temperature T' and external voltage u_S can be adjusted to estimate the dependence of firing modes on these intrinsic parameters, and the phototube can be activated as a stable voltage source. For simplicity, the voltage can be adjusted as a combination of constant and periodical terms in the form $u_S = u_0 + A\cos\omega\tau$. On the other hand, the photocurrent can be regarded as a stable current source, and this neural circuit is driven by time-varying current with certain saturation. The neuron oscillator is described by

$$\begin{cases} \dfrac{\mathrm{d}x}{\mathrm{d}\tau} = x - \dfrac{1}{3}x^3 - y + i_S, \\ \dfrac{\mathrm{d}y}{\mathrm{d}\tau} = c[x + a - b(T')y]. \end{cases} \tag{7}$$

In addition, the photocurrent defined in Eq. (4) can be approached by

$$i_S = I_0 \mathrm{arctg}(x - v_a), \tag{8}$$

where I_0 is the maximal value for dimensionless photocurrent and the normalized threshold v_a is associated with the material property of the cathode in the phototube. In this neural circuit, field energy is propagated and pumped between the capacitor and induction coil, and the field energy can be obtained by

$$W = \frac{1}{2}CV^2 + \frac{1}{2}Li_L^2 = CV_0^2\left(\frac{1}{2}x^2 + \frac{1}{2}cy^2\right) = CV_0^2 H. \tag{9}$$

By applying the same scale transformation for the field energy, the Hamilton energy is calculated by

$$H = \frac{1}{2}x^2 + \frac{1}{2}cy^2. \tag{10}$$

As is well known, the resistance of the thermistor is dependent on the temperature. In fact, the temperature for the thermistor could be time-varying because the Joule heat can be accumulated when the channel current passes through the thermistor in the neural circuit. For simplicity, the temperature of the thermistor is controlled by

$$T'(\tau) = \begin{cases} 0.00008\tau^2 + 5, & 0 < \tau \leqslant 500, \\ 10\cos\omega\tau + 25, & 500 < \tau \leqslant 1000, \\ -0.00008(\tau - 1000)^2 + 25, & 1000 < \tau \leqslant 1500. \end{cases} \tag{11}$$

In the successive section, these parameters will be controlled to trigger firing patterns with different oscillation modes, and bifurcation analysis is carried out for detecting mode transition dependence on the parameters and external excitation.

3. Results and discussion

For nonlinear analysis, the fourth order Runge–Kutta algorithm is applied to find numerical solutions for Eqs. (6), (7), and (10). The time step and initial values for the variables are selected as 0.001 and (0.1, 0.3). For simplicity, in the numerical studies, the dimensionless time τ is replaced by t in the figures for presenting sampled time series. At first, we consider the case when the phototube is used as voltage source $u_S = u_0 + A\cos\omega\tau$, and the temperature is adjusted to detect the mode selection and transition in the neural activities. The formation of attractors and evolution of outputs are shown in Figs. 2 and 3 when the temperature is fixed at certain constants.

By taming the amplitude of the voltage source, the neural circuit can present firing patterns in periodical and/or chaotic modes when the temperature is fixed. Furthermore, the temperature is decreased and the resistance of the thermistor is increased to change the branch current, and the results are shown in Fig. 3.

It is found that a stable periodical oscillation can be induced by adjusting the temperature and amplitude in the photocurrent. The sampled time series are further calculated to estimate the dependence of firing modes on the amplitude of the signal source, and the bifurcation analysis is presented in Fig. 4.

Indeed, the firing pattern and oscillation modes are dependent on the temperature greatly. In case of lower temperature, the resistance of the thermistor is high and the branch channel current is blocked to prevent possible exciting on the neural circuit. When the temperature of the thermistor is increased, appropriate setting for the amplitudes of the voltage source can induce distinct mode transition from periodical type to bursting, and chaotic states completely. Furthermore, the angular frequency of the voltage source is adjusted to detect possible occurrence of mode transition, and then the phase portraits are plotted in Fig. 5.

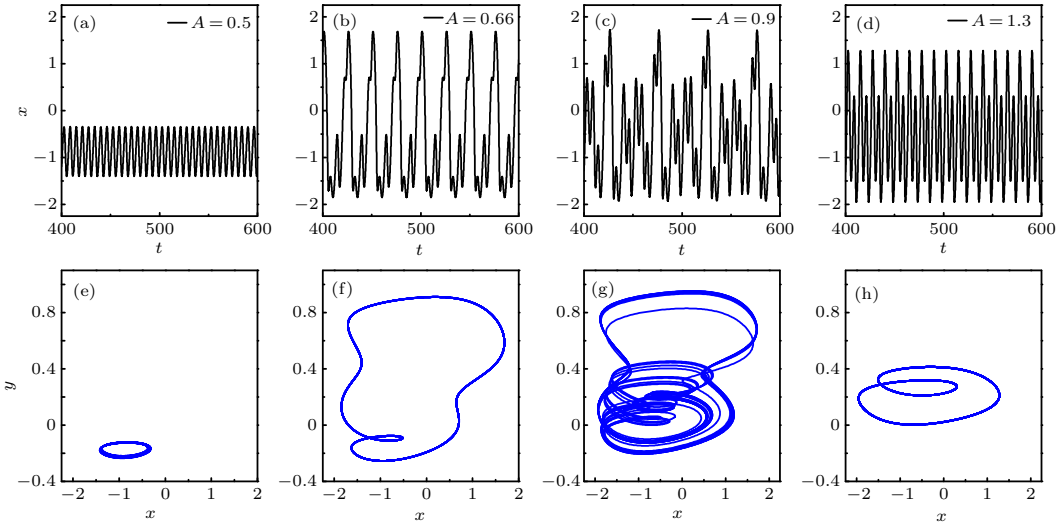

Fig. 2. Sampled time series for variable x and formation of attractors: (a), (e) $A = 0.5$; (b), (f) $A = 0.66$; (c), (g) $A = 0.9$; (d), (h) $A = 1.3$, and the parameters are fixed at $T' = 5$, $u_0 = 0.2$, $\omega = 1.004$, $b_0 = 0.8$, $a = 0.7$, $c = 0.1$, $\xi = 0.175$. b_0 is the maximal resistance of the thermistor.

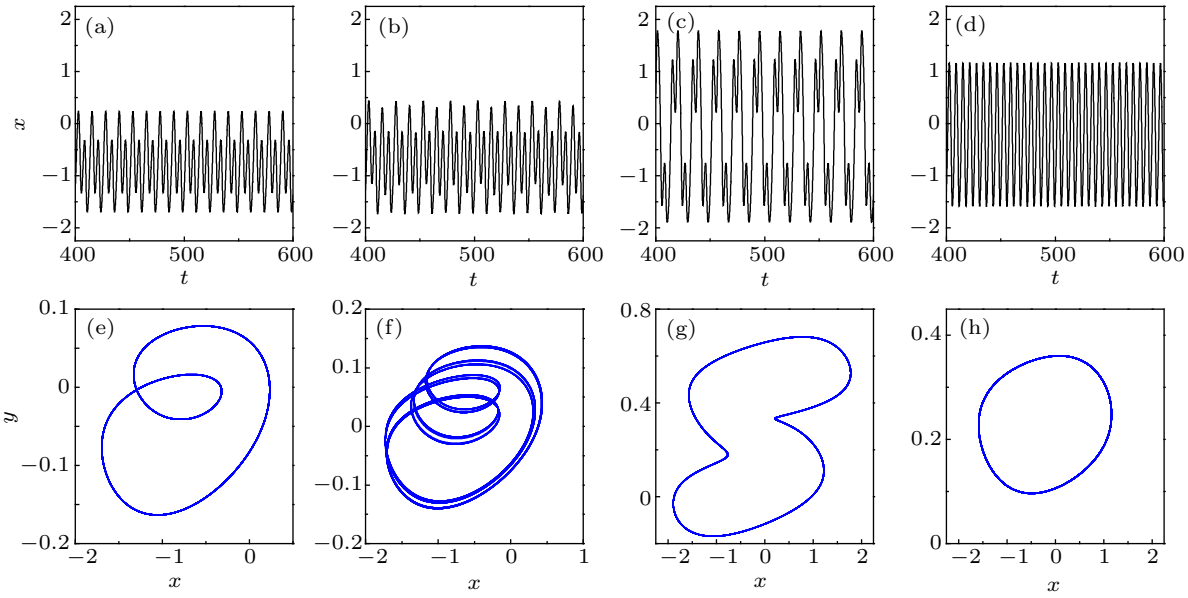

Fig. 3. Sampled time series for variable x and formation of attractors: (a), (e) $A = 0.76$; (b), (f) $A = 0.83$; (c), (g) $A = 0.99$; (d), (h) $A = 1.36$, and the parameters are fixed at $T' = 1$, $u_0 = 0.2$, $\omega = 1.004$, $b_0 = 0.8$, $a = 0.7$, $c = 0.1$, $\xi = 0.175$. b_0 is the maximal resistance of the thermistor.

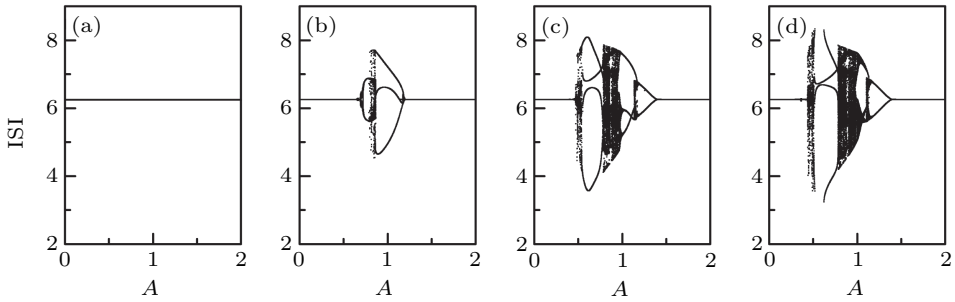

Fig. 4. Bifurcation diagram is calculated by detecting interspike intervals (ISIs) from the sampled time series for the variable x when the amplitude of voltage source is changed: (a) $T' = 0.5$; (b) $T' = 1$; (c) $T' = 5$; (d) $T' = 20$, and the parameters are fixed at $u_0 = 0.2$, $\omega = 1.004$, $b_0 = 0.8$, $a = 0.7$, $c = 0.1$, $\xi = 0.175$.

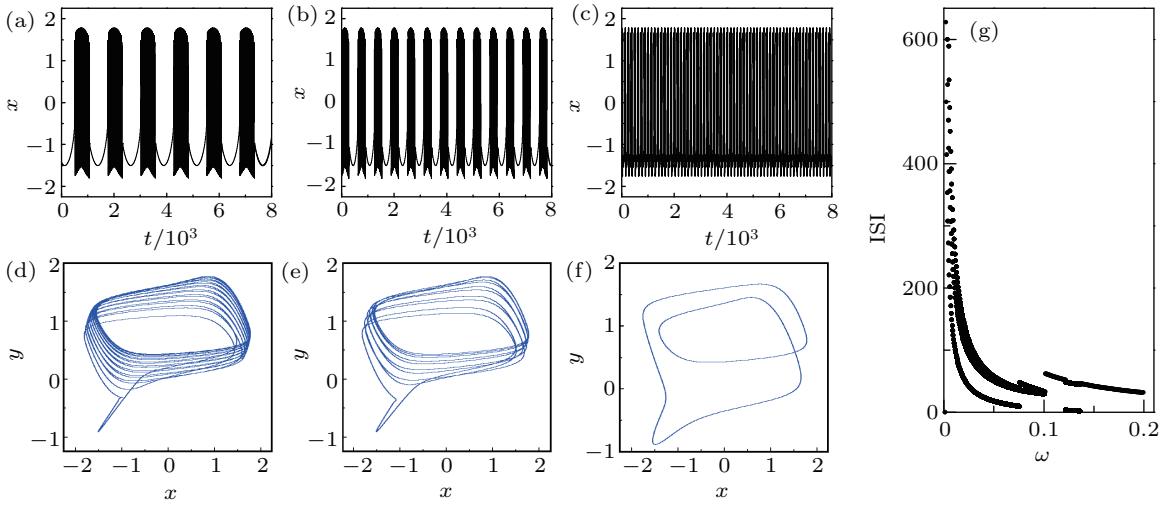

Fig. 5. (a)–(c) Sampled time series for variable x, (d)–(f) formation of attractors, and (g) bifurcation diagram vs. angular frequency. For (a), (d) $\omega = 0.005$; (b), (e) $\omega = 0.01$; (c), (f) $\omega = 0.05$, and the parameters are fixed at $T' = 10$, $A = 1$, $u_0 = 0.2$, $b_0 = 0.8$, $a = 0.7$, $c = 0.1$, $\xi = 0.175$.

That is, the formation of attractors and firing patterns are also dependent on the frequency of the voltage source. The neural circuit can present distinct bursting and then it is tamed to trigger periodical firing. Extensive results confirm that periodical oscillation can be enhanced to generate chaotic firing by adjusting the frequency in the voltage source. Therefore, more bifurcation calculation is carried out, and the results are shown in Fig. 6.

Within a finite frequency range, it is confirmed that chaotic firing can be induced while periodical firing can be

generated by taming the frequency of the voltage source in a wide range. Also, the dependence of firing pattern on thermistor temperature is estimated by calculating the bifurcation diagram in Fig. 7.

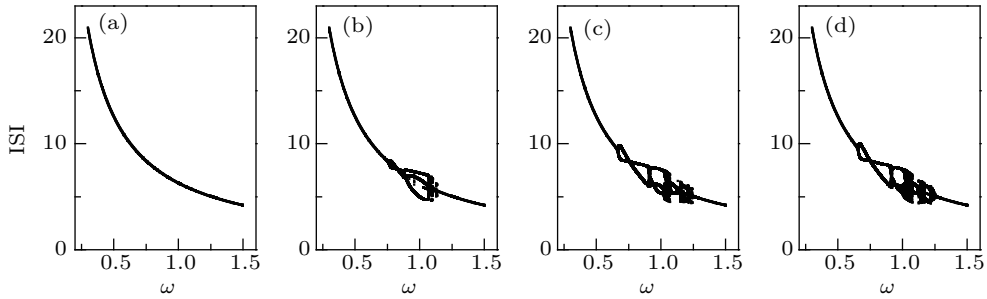

Fig. 6. Bifurcation diagram is calculated by detecting ISIs from the sampled time series for the variable x when the frequency of voltage source is changed: (a) $T' = 0.5$; (b) $T' = 1$; (c) $T' = 5$; (d) $T' = 10$, and the parameters are fixed at $u_0 = 0.2$, $A = 1$, $b_0 = 0.8$, $a = 0.7$, $c = 0.1$, $\xi = 0.175$.

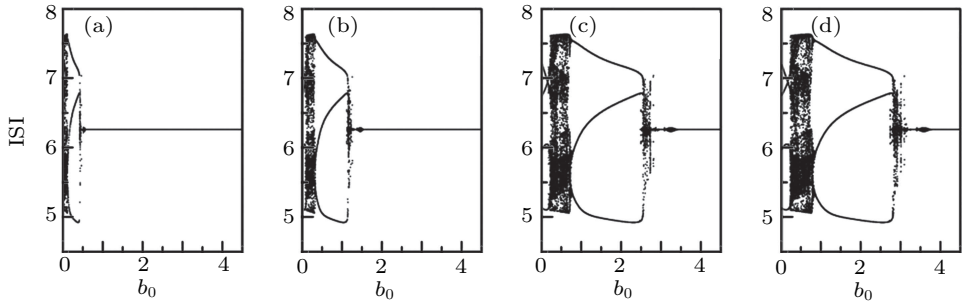

Fig. 7. Bifurcation diagram is calculated by detecting ISIs from the sampled time series for the variable x when the amplitude of thermistor is changed: (a) $T' = 0.5$; (b) $T' = 1$; (c) $T' = 5$; (d) $T' = 10$, and the parameters are fixed at $u_0 = 0.2$, $A = 1$, $\omega = 1.004$, $b_0 = 0.8$, $a = 0.7$, $c = 0.1$, $\xi = 0.175$.

In Fig. 7, it is demonstrated that the parameter region for generating chaotic states can be extended when the temperature of the thermistor is increased. Distinct mode transition from chaotic state to periodical one occurs, and then it can recovery to chaotic oscillation by changing the resistance of the thermistor. Extensive numerical calculation is applied, stable chaotic attractors can be formed at $b_0 = 0.6$, 0.7 while $b_0 = 0.8$, 0.9 can support the survival of periodical attractors when the parameters are fixed at $u_0 = 0.2$, $A = 1$, $\omega = 1.004$, $T' = 13.5$, $b_0 = 0.8$, $a = 0.7$, $c = 0.1$, $\xi = 0.175$. Furthermore, bifurcation analysis is presented to find dependence of firing modes on the temperature for the thermistor, and the temperature-induced bifurcation and mode transition are shown in Fig. 8.

The maximal resistance of the thermistor has distinct effect on the firing patterns and mode selection, and it is controlled by the intrinsic physical property of material. It is also important to discuss the case when the temperature of the thermistor is changed continuously, and the Hamilton energy is also calculated to find the dependence of energy release on firing patterns, the results are presented in Fig. 9.

It is confirmed that slight changes in the temperature can induce distinct response in the thermistor, as a result, the firing patterns show rapid transition and then the Hamilton energy in periodical oscillation is decreased to release energy for supporting a chaotic firing. Therefore, this neural circuit becomes sensitive to slight changes in the temperature of the thermistor. In addition, the amplitude and frequency of the voltage source can be further tamed to detect the occurrence of other firing patterns and mode transition.

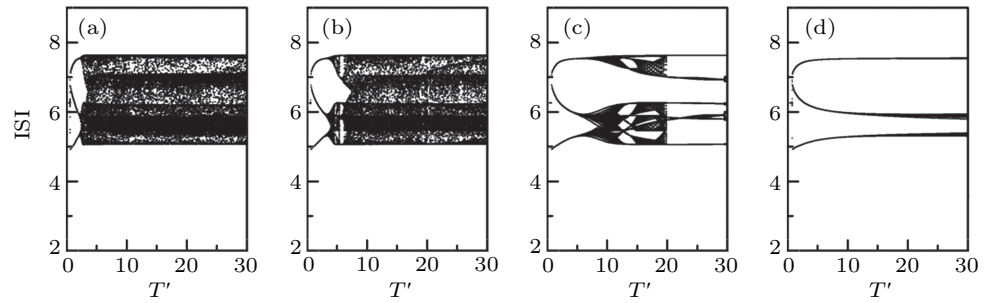

Fig. 8. Bifurcation diagram is calculated by detecting ISIs from the sampled time series for the variable x when the temperature for thermistor is changed: (a) $b_0 = 0.6$; (b) $b_0 = 0.7$; (c) $b_0 = 0.8$; (d) $b_0 = 0.9$, and the parameters are fixed at $u_0 = 0.2$, $A = 1$, $\omega = 1.004$, $a = 0.7$, $c = 0.1$, $\xi = 0.175$.

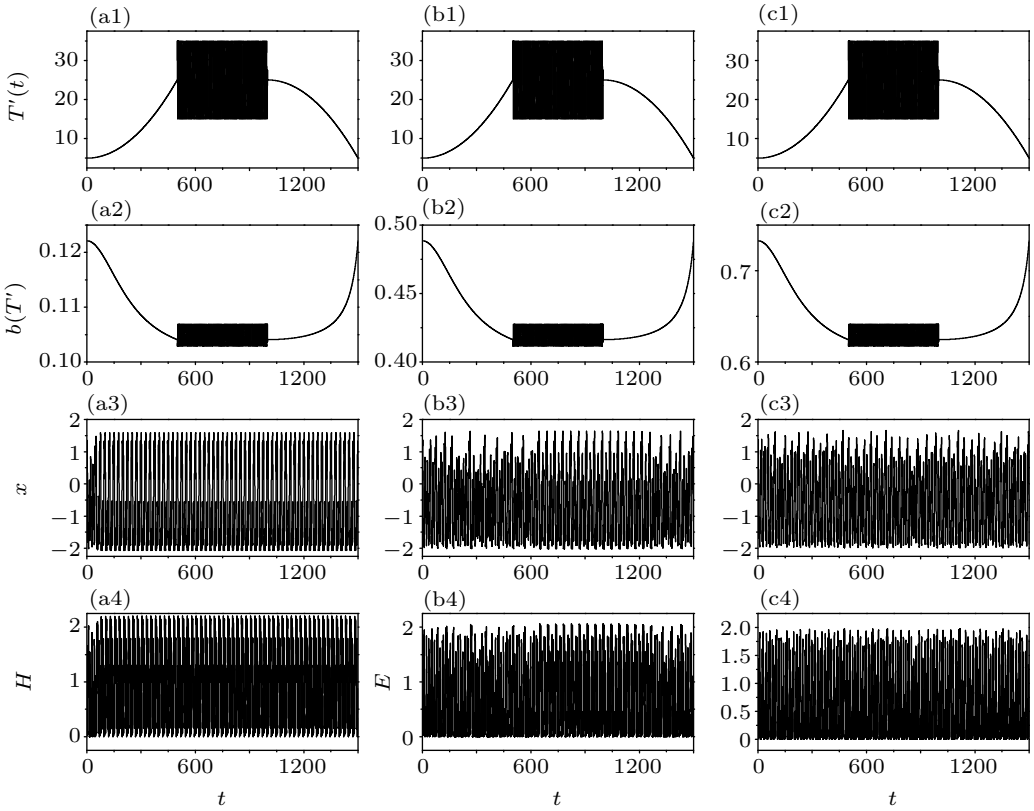

Fig. 9. Correlation between temperature, resistance of thermistor, firing patterns and Hamilton energy are calculated by changing the temperature of the thermistor. For (a1)–(a4) $b_0 = 0.1$; (b1)–(b4) $b_0 = 0.4$; (c1)–(c4) $b_0 = 0.6$, and the parameters are fixed at $u_0 = 0.2$, $A = 1$, $\omega = 1.004$, $a = 0.7$, $c = 0.1$, $\xi = 0.175$.

Interestingly, the second case is discussed when the phototube is used as a stable current source, and the photocurrent is defined in Eq. (8). The output voltage of the neural circuit is adjusted by the time-varying photocurrent, and the evolution of firing patterns is presented in Fig. 10.

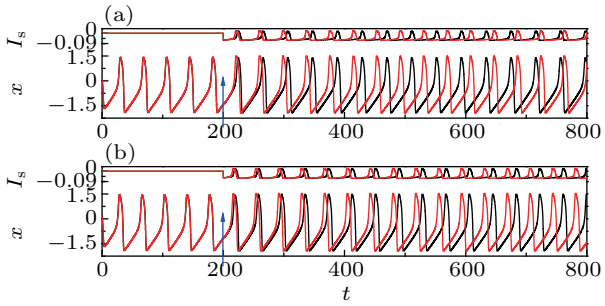

Fig. 10. Firing pattern and photocurrent are calculated as functions of time by applying different temperatures for the thermistor. For (a) $T' = 10$; (b) $T' = 30$, and the parameters are fixed at $I_0 = 0.05$, $b_0 = 0.3$, $a = 0.7$, $c = 0.1$, $\xi = 0.175$, $v_a = 1$ (black line), $v_a = 0.1$ (red line). The photocurrent is released from $t = 200$ time units.

The results in Fig. 10 demonstrate that the excitation of photocurrent depends on the inverse cut-off threshold v_a, and the stimulus from the current source is blocked when the threshold v_a is much small. The potential mechanism is that the change of photocurrent can regulate the excitability of neuron and thus the dynamics is controlled completely. In experimental way, the intensity of external light and illumination can be changed in the amplitude and frequency, as a result, the

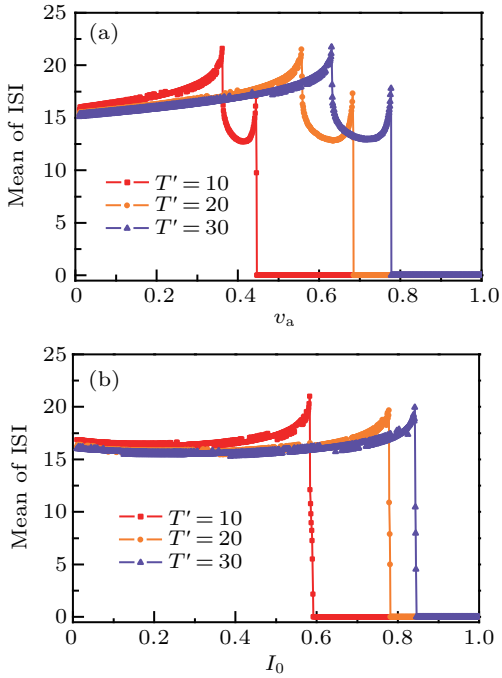

Fig. 11. Mean duration of spiking is calculated by changing the parameters (I_0, T') with $b_0 = 0.3$, $T' = 10$ (red line-square), $T' = 20$ (orange line-circle), $T' = 30$ (violet line-up triangle). For (a) $I_0 = 0.1$; (b) $v_a = 0.1$.

photocurrent can be adjusted freely. When the temperature for the thermistor is changed, the similar results are confirmed and the neural circuit is excited for presenting periodical firing. Furthermore, the amplitude of photocurrent is increased to detect the firing patterns, and the results confirm that the

amplitude in the firing series is decreased greatly. Therefore, the temperature for the thermistor and the amplitude of the photocurrent are synchronously changed to trigger mode transition in neural activities, and the average duration of spiking is calculated in Fig. 11.

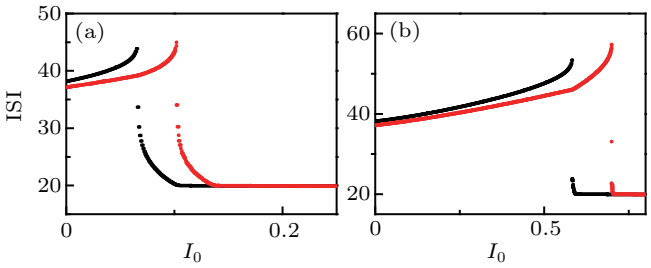

Fig. 12. Bifurcation diagram is calculated by detecting ISIs from the sampled time series for the variable x when the amplitude for photocurrent is changed. For (a) $v_a = 1.0$; (b) $v_a = 0.1$, and the parameters are fixed at $b_0 = 0.3$, $T' = 10$ (black dots), $T' = 30$ (red dots), $a = 0.7$, $c = 0.1$, $\xi = 0.175$.

It is found that the phase of the firing patterns is much dependent on the amplitude and inverse voltage threshold in the photocurrent across the phototube. Extensive bifurcation analysis is carried out, and the results are plotted in Figs. 12 and 13 by calculating the dependence of ISIs on the amplitude I_0 and threshold v_a in the photocurrent.

From the results in Fig. 12, it is found that the firing mode can be tamed effectively by regulating the intrinsic parameter v_a and the amplitude of photocurrent in the phototube. Furthermore, the mode transition of neural activities induced by the cut-off voltage parameter is estimated by keeping the temperature, and the results are shown in Fig. 13.

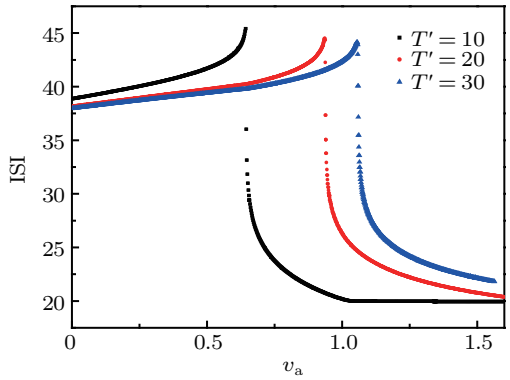

Fig. 13. Bifurcation diagram is calculated by detecting ISIs from the sampled time series for the variable x when the inverse threshold for photocurrent is changed. The parameters are fixed at $b_0 = 0.3$, $I_0 = 0.2$, $T' = 10$ (black dots), $T' = 20$ (red dots), $T' = 30$ (blue dots), $a = 0.7$, $c = 0.1$, $\xi = 0.175$.

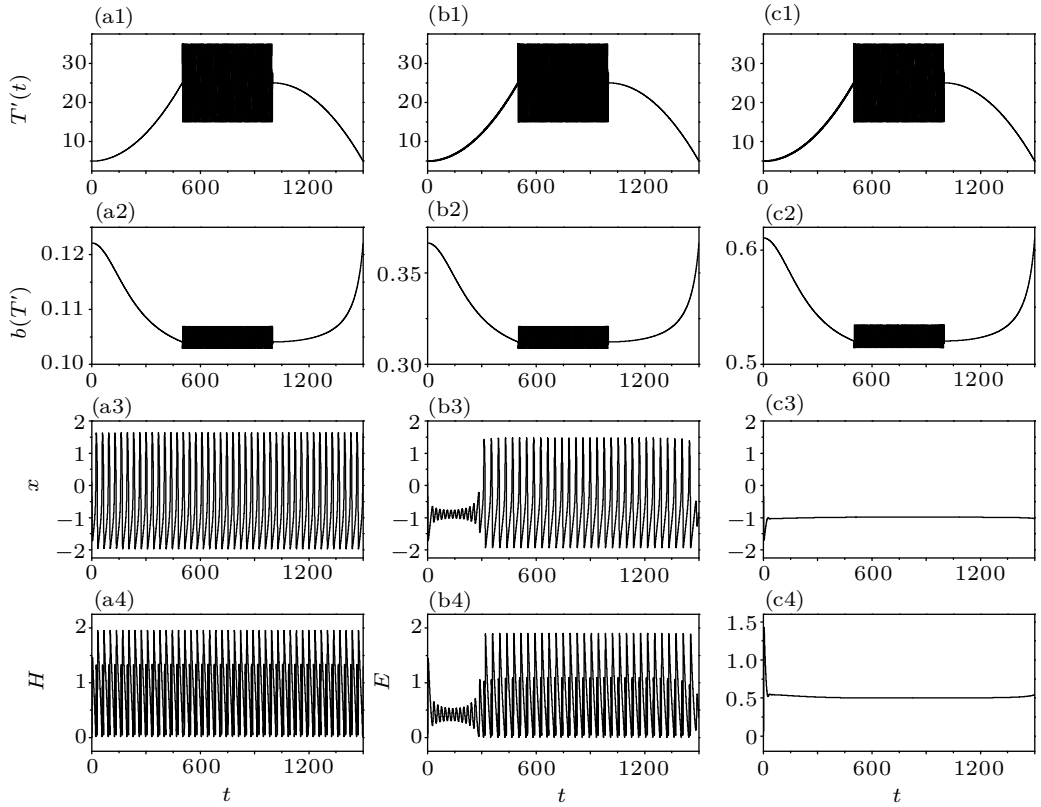

Fig. 14. Correlation between temperature, resistance of thermistor, firing patterns and Hamilton energy are calculated by changing the temperature for the thermistor. For (a1)–(a4) $b_0 = 0.1$; (b1)–(b4) $b_0 = 0.3$; (c1)–(c4) $b_0 = 0.5$, and the parameters are fixed at $I_0 = 0.05$, $v_a = 1.0$, $a = 0.7$, $c = 0.1$, $\xi = 0.175$.

The results in Fig. 13 confirm that the temperature for the thermistor has distinct impact on the firing patterns and distinct phase transition is induced with the increase of parameter v_a. Indeed, when the intrinsic parameter v_a is kept at lower value, the current source can be blocked due to higher value of the membrane potential (output voltage of the capacitor). The current source releases its function when v_a is kept at higher value because the membrane potential is below this threshold

and the neuron can be excited continuously. It is interesting to analyze the mode transition when the temperature of the thermistor is changed with time, and the results are shown in Fig. 14.

The membrane potential of neuron is regulated by changing the temperature of the thermistor, which can adjust the branch current and the energy propagation in the neural circuit. When the resistance of the thermistor is increased, the channel current across the thermistor is decreased and then the oscillation mode in the neural circuit is suppressed to trigger quiescent state. It is interesting to investigate whether similar bursting patterns can be induced when the temperature of the thermistor is adjusted with periodical fluctuation, and the results are shown in Fig. 15.

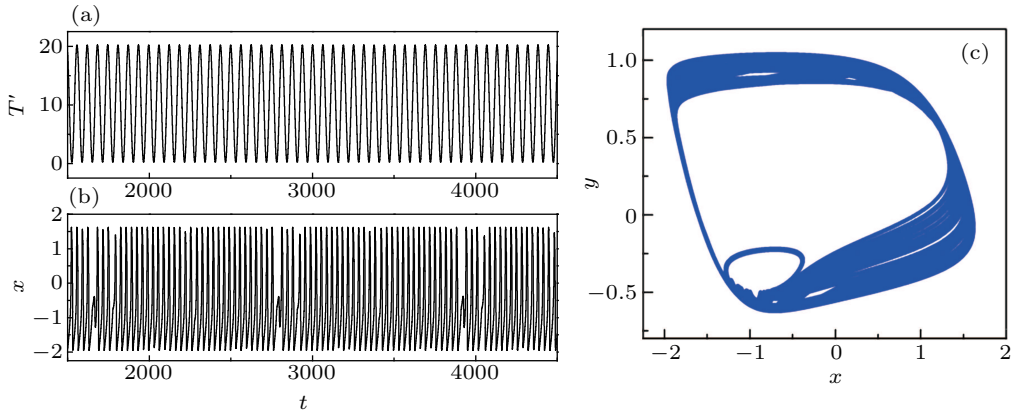

Fig. 15. (b) Sampled time series for the variable x and (c) attractor are calculated when the temperature for the thermistor is adjusted as (a) $T' = 10.2 + 10\cos 0.1001\tau$. The parameters are selected as $a = 0.7$, $c = 0.1$, $\xi = 0.175$, $I_S = 0.0$, $b_0 = 0.01$.

It is confirmed that bursting pattern can be induced in the neural activities and continuous switch between periodical orbit and chaotic orbits can be triggered even the photocurrent is blocked completely. Furthermore, the firing pattern is controlled when the photocurrent from the phototube is released. Indeed, when the photocurrent in Eq. (4) is mapped into dimensionless photocurrent in Eq. (8) by applying $V \to V/V_0 = x$, the scale factor is selected as $V_0 = 1$ to get a simple form for the current source. In fact, it can be replaced by a generic form as $V/V_0 = kx$. In Fig. 16, the output variable x is calculated by supplying certain value for the scale factor k.

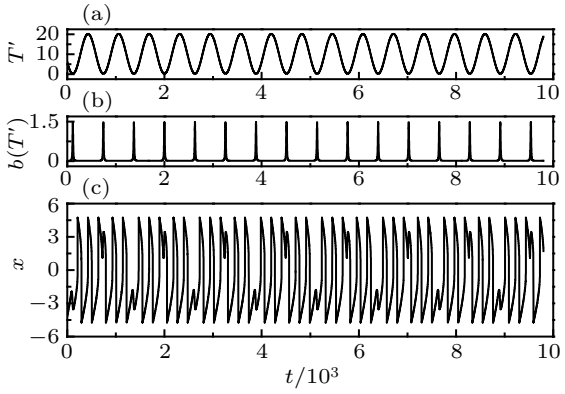

Fig. 16. (c) Sampled time series for the variable x and (b) resistance of thermistor are calculated when the temperature for thermistor is adjusted as (a) $T' = 10.2 + 10\cos 0.01\tau$. The parameters are selected as $a = 0.7$, $c = 0.1$, $\xi = 0.175$, $I_S = 10\arctan(25x - 10)$, $b_0 = 0.01$.

That is, slight fluctuation in the thermistor temperature is effective to regulate the firing pattern of neuron driven by photocurrent. In practical way, when the temperature of the thermistor and photocurrent are perturbed with stochastic disturbance, the firing modes could be more complex.

As is well known, neuron can present the main property of excitable media. In generic way, artificial neurons and intelligent circuits can be tamed to present quiescent, spiking, bursting, and chaotic states, which are the main dynamical properties of biological neuron by adjusting the signal source and intrinsic parameters. In absence of external periodic stimulus, coherence resonance[68–70] can be induced by changing the excitability and noise. When noise is imposed on the network, spatial coherence resonance[71–73] can be induced by taming the local kinetics and noise intensity. For simplicity, Gaussian white noise is imposed on this functional neuron. The coefficient variability (CV) of ISI series is calculated to estimate the coherence degree as follows:

$$CV = \frac{\sqrt{\langle \bar{T}^2 \rangle - \langle \bar{T} \rangle^2}}{\langle \bar{T} \rangle}; \tag{12}$$

where $\bar{T}$ denotes the average ISI and it indicates higher coherence degree when CV is kept with smaller value. Noise is a kind of stochastic signal and can be imposed on the neuron for detecting possible occurrence of stochastic resonance and coherence. The statistical properties of Gaussian white noise are defined by

$$\langle \zeta(t) \rangle = 0, \quad \langle \zeta(t)\zeta(t') \rangle = 2D\delta(t - t'), \tag{13}$$

where D is the noise intensity and it can be adjusted to induce coherence resonance and enhance the regularity of the firing patterns of neuron. For further confirming the excitable property in this functional neuron, Gaussian white noise in additive type is imposed on the neural circuit, and coherence resonance is detected when the neural circuit is driven by voltage source

and current source, respectively. It is confirmed that similar coherence resonance can be induced by applying appropriate noise intensity no matter whether the phototube is considered as voltage source or current source. The results are plotted in Figs. 17 and 18.

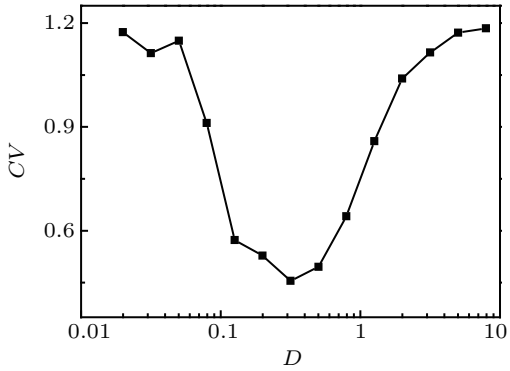

Fig. 17. Coefficient variability of ISI series is calculated by changing the noise intensity when the phototube is used as voltage source. The parameters are fixed at $a = 0.7$, $c = 0.1$, $\xi = 0.175$, $u_0 = 0.2$, $A = 0.76$, $\omega = 1.004$, $b_0 = 0.8$, $T' = 1$. During getting the average ISI, the threshold for peaks is selected as 0.3.

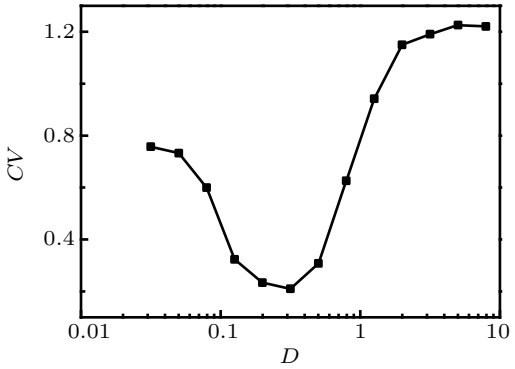

Fig. 18. Coefficient variability of ISI series is calculated by changing the noise intensity when the phototube is used as current source. The parameters are fixed at $a = 0.7$, $c = 0.1$, $\xi = 0.175$, $I_0 = 0.19$, $\nu_a = 1$, $b_0 = 0.3$, $T' = 10$. During getting the average ISI, the threshold for peaks is selected as 0.3.

As shown in Figs. 17 and 18, the involvement of noise can regulate the coherence of the time series of membrane potentials. When other parameters are fixed, appropriate noise intensity can be detected for enhance the coherence degree when smaller CV value is stabilized. Extensive numerical results can be applied to confirm that noise can active quiescent neuron for generating spiking, bursting, and chaotic firing patterns. For simplicity, Gaussian white noise is considered in this functional neuron, while Lévy noise, colored noise, and others[74–78] can also be imposed to find new attractive phenomena similar to the stochastic and coherence resonance in other excitable media. For example, Valenti *et al.*[79] discussed the dynamics of the Fitz–Hugh–Nagumo (FHN) model in the presence of colored noise and a periodic signal, and they explored the meaningful modifications of the resonant activation (RA) and noise enhanced stability (NES) phenomena due to the correlation time of the noise.

In a summary, functional electronic components can be included into generic nonlinear circuits for reproducing similar firing patterns and neural activities in biological neurons by regulating the intrinsic parameters of these physical components carefully. A nonlinear circuit can be tamed to present quiescent, spiking, bursting, and chaotic firing patterns and then the main dynamical properties of biological neurons can be reproduced. The involvement of thermistor can estimate the temperature effect on ion channels while the involvement of phototube can detect the effect of external illumination and electromagnetic radiation. As a result, more phototubes can be used as signal source when they are activated to trigger continuous photocurrents for the circuits. For extensive discussion, readers can investigate the synchronization stability between neurons coupled with electronic synapse and/or chemical synapse.[80,81]

As is well known, fever can cause coma and the nervous system shows disorder. It is interesting to clarify the potential biophysical mechanism by exploring the dynamics of the thermosensitive neuron, which can be mapped from a functional neural circuit. It also can be treated as smart sensor and auxiliary component in the application of fault diagnosis and fuzzy control[82–84] in complex systems. As suggested in the review,[85,86] more physical components can be included into the neural circuits and field coupling is triggered to balance the energy pumping in the networks.

4. Open problems

Biological neurons have complex anatomies and specific functions are developed to encode different kinds of external stimuli. External light and optical signals can be encoded by eyes and equivalent currents are generated to stimulus the visual nervous system, and right gaits can be kept. It is a challenge to discover the biophysical process how light stimulus is converted into current stimulus across the visual cells. Inspired by the physical properties of phototube, in which illumination can be converted into photocurrent, phototube can be used to drive the neural circuit by generating continuous currents. The activation of cells depends on the ambient temperature[62] because the conductance of channels of cells and gate variables can be changed to regulate the channel current. In the Hodgkin-Huxley neuron,[87,88] a scale factor is introduced as follows:

$$\Phi(T) = 3^{(T-6.3\ ^\circ\mathrm{C})/10\ ^\circ\mathrm{C}}. \tag{14}$$

The voltage-dependent opening and closing rate functions are multiplied by the scale factor, and the gate variables are adjusted to regulate the membrane potential of neurons. However, it becomes difficult and useless when the neuron models contain no channel variables. Therefore, we suggest that

thermistor can be used to estimate the heat effect and temperature because then the channel current across the thermistor and branch circuit can be regulated by the temperature effectively. Our suggestion and proposal for this functional neuron model can shed light on obtaining more functional neural circuits by utilizing the physical properties of more electronic components, and it also give possible insights to understand the biophysical mechanism for encoding external physical signals in neurons. The physical components such as phototube and thermistor are involved, while the authors seldom consider the realistic parameters values in these commercial devices. In fact, the same analog circuits and their realization in hardware can be tried in the forthcoming experiments.

To enhance the dependence and sensitivity of temperature, more thermistor can be included into the circuit, e.g., thermistor can be connected to the phototube, and more phototubes can be paralleled to increase the intensity of photocurrent as well. In addition, more physical components can be included to enhance its biophysical function. For researchers in the field of computational neuroscience, they can use this functional neuron model for further bifurcation analysis, estimating the network stability under more stimuli and spatial coherence resonance if possible.

As suggested in Ref. [31], memristor can be involved to describe the memristive synapse and induction current in the neuron due to electromagnetic induction. That is, magnetic flux can be involved into the neuron models for estimating the mode transition and dynamics in neural activities, for example, Ref. [89] investigated the effect of electromagnetic radiation and external forcing current on the pre-Bötzinger complexity in mammalian brainstem and the transition in the generation of respiratory rhythms was discussed. Qu *et al.*[90] discussed the effect of stochastic electromagnetic disturbances on neurons driven by autapse. Yuan *et al.*[91] studied a simple neuron-astrocyte coupled system under electromagnetic induction in response to different types of external stimulation, and it was confirmed that the duration and intensity of the external stimulus can induce different modes of electrical activity in this system, and thus the neuronal firing patterns can be subtly controlled. The biological neurons can be tamed to obtain main functions after continuous self-learning and training. In practical way, more functional electronic components can be combined to build functional neurons, which can capture and percept the external light, heat, mechanical pressure, voice, and even magnetic field. When these artificial neurons are obtained, they can be connected to build multi-layer networks and cooperation between different functional regions of brain can be estimated in a possible way. Also, some researchers can confirm these suggestions by implementing analog, digital circuits and even realization in hardware if possible.

5. Conclusions

In this paper, two physical electronic components are used to enhance the intelligent function of the neural circuit and a feasible neuron model is proposed to estimate the effect of temperature and illumination. The photocurrent across phototube can excite the neural circuit as signal source (voltage source and/or current source). The thermistor in this neural circuit is sensitive to the temperature and heat effect because the channel current across the thermistor can be adjusted by temperature.

Standard bifurcation analysis is applied to find the dynamics dependence on the temperature and photocurrent. The external illumination energy can be encoded by generating photocurrent, and fluctuation in the temperature can be detected by changing the channel current. In addition, Gaussian white noise is imposed on this neuron, and the occurrence of coherence resonance is confirmed by applying appropriate noise intensity. This functional neural circuit can be further used for artificial neural network and sensors. It also explains the biophysical mechanism how temperature (heat) and light can encoded in the nervous system.

References

[1] Schwiening C J 2012 *J. Physiol.* **590** 2571
[2] Hindmarsh J L and Rose R M 1984 *Proc. R. Soc. B Biol. Sci.* **221** 87
[3] Jia B, Gu H G and Xue L 2017 *Cogn. Neurodyn.* **11** 189
[4] Zhu F, Wang R, Pan X, *et al.* 2019 *Cogn. Neurodyn.* **13** 75
[5] Wu F, Ma J, Zhang G, *et al.* 2019 *Appl. Math. Comput.* **347** 590
[6] Wu F, Ma J, Zhang G, *et al.* 2020 *Sci. Chin. Technol. Sci.* **63** 625
[7] Cunningham M O, Whittington M A, Bibbig A, *et al.* 2004 *Proc. Natl. Acad. Sci. USA* **101** 7152
[8] Wu J and Ma S 2019 *Nonlin. Dyn.* **96** 1895
[9] Han X, Bi Q, Ji P, *et al.* 2015 *Phys. Rev. E* **92** 012911
[10] Han X, Liu Y, Bi Q, *et al.* 2019 *Commun. Nonlin. Sci. Numer. Simulat.* **72** 16
[11] Allen N J and Eroglu C 2017 *Neuron* **96** 697
[12] Chung W, Allen N J, Eroglu C, *et al.* 2015 *CSH Perspect. Biol.* **7** a020370
[13] Vasile F, Dossi E, Rouach N, *et al.* 2017 *Brain Struct. Funct.* **222** 2017
[14] Huguet G, Joglekar A, Messi L M, *et al.* 2016 *Biophys. J.* **111** 452
[15] Tang J, Zhang J, Ma J, *et al.* 2017 *Sci. Chin. Technol. Sci.* **60** 1011
[16] Guo S, Tang J, Ma J, *et al.* 2017 *Complexity* **2017** 4631602
[17] Wang C, Guo S, Xu Y, *et al.* 2017 *Complexity* **2017** 5436737
[18] Bekkers J M 2003 *Curr. Biol.* **13** R433
[19] Yue Y, Liu L, Liu Y, *et al.* 2017 *Nonlin. Dyn.* **90** 2893
[20] Uzun R, Yilmaz E, Ozer M, *et al.* 2017 *Physica A* **486** 386
[21] Yilmaz E, Baysal V, Ozer M, *et al.* 2016 *Physica A* **444** 538
[22] Yang X L, Yu Y H and Sun Z K 2017 *Chaos* **27** 083117
[23] Gong Y B, Wang B Y and Xie H J 2016 *Biosyst.* **150** 132
[24] Song X L, Wang C N, Ma J, *et al.* 2015 *Sci. Chin. Technol. Sci.* **58** 1007
[25] Song X, Wang H, Chen Y, *et al.* 2019 *Nonlin. Dyn.* **96** 2341
[26] Song X, Wang H, Chen Y, *et al.* 2018 *Nonlin. Dyn.* **94** 141
[27] Zhao Z and Gu H 2017 *Sci. Rep.* **7** 6760
[28] Kim Y, Park J and Choi Y K 2019 *Antioxidants* **8** 121
[29] Wang C and Ma J 2018 *Int. J. Mod. Phys. B* **32** 1830003
[30] Ma J, Yang Z, Yang L, *et al.* 2019 *J. Zhejiang Univ. Sci. A* **20** 639
[31] Ma J and Tang J 2015 *Sci. Chin. Technol. Sci.* **58** 2038
[32] Chua L O 2011 *Appl. Phys. A* **102** 765
[33] Wang Z, Joshi S, Savelev S, *et al.* 2017 *Nat. Mater.* **16** 101
[34] Muthuswamy B 2010 *Int. J. Bifur. Chaos* **20** 1335
[35] Kim H, Sah M P, Yang C, *et al.* 2012 *IEEE Tr. Circ. Syst.* **59** 2422
[36] Xu F, Zhang J, Fang T, *et al.* 2018 *Nonlin. Dyn.* **92** 1395
[37] Serb A, Corna A, George R, *et al.* 2020 *Sci. Rep.* **10** 2590

[38] Park S, Chu M, Kim J, *et al.* 2015 *Sci. Rep.* **5** 10123
[39] Bao H, Zhang Y, Liu W, *et al.* 2020 *Nonlin. Dyn.* **100** 937
[40] Lu L, Jia Y, Xu Y, *et al.* 2019 *Sci. Chin. Technol. Sci.* **62** 427
[41] Jin W, Wang A, Ma J, *et al.* 2019 *Sci. Chin. Technol. Sci.* **62** 2113
[42] Ge M, Lu L, Xu Y, *et al.* 2019 *Euro. Phys. J.-Spec. Top.* **228** 2455
[43] Xu Y, Jia Y, Wang H, *et al.* 2019 *Nonlin. Dyn.* **95** 3237
[44] Usha K and Subha P A 2019 *Nonlin. Dyn.* **96** 2115
[45] Guo S, Xu Y, Wang C, *et al.* 2017 *Chaos Solitons & Fractals.* **105** 120
[46] Qin H, Wang C, Cai N, *et al.* 2018 *Physica A* **501** 141
[47] Abdelouahab M, Lozi R, Chua L O, *et al.* 2014 *Int. J. Bifur. Chaos* **24** 1430023
[48] Xu Y M, Yao Z, Hobiny A, *et al.* 2019 *Front. Inform. Technol. Electron. Eng.* **20** 571
[49] Wickramasinghe M and Kiss I Z 2013 *Phys. Rev. E* **88** 062911
[50] Yao Z, Ma J, Yao Y, *et al.* 2019 *Nonlin. Dyn.* **96** 205
[51] Pavlov A, Steur E, De Wouw N V, *et al.* 2009 *Conference on decision and control* pp. 5263–5268
[52] Liu Z, Wang C, Zhang G, *et al.* 2019 *Int. J. Mod. Phys. B* **33** 1950170
[53] Gambuzza L V, Buscarino A, Fortuna L, *et al.* 2015 *IEEE Tr. Circ. Syst. I* **62** 1175
[54] Gambuzza L V, Frasca M, Fortuna L, *et al.* 2017 *IEEE Tr. Circ. Syst. I* **64** 2124
[55] Zhang X, Wu F, Ma J, *et al.* 2020 *AEU-Int. J. Electron. Commun.* **115** 153050
[56] Zhang Y, Wang C N, Tang J, *et al.* 2020 *Sci. Chin. Technol. Sci.*
[57] Xu W and Sudhof T C 2013 *Science* **339** 1290
[58] Landahl H D and Householder A S 1939 *Psychometrika* **4** 255
[59] Yonezu H, Miho A, Himeno T, *et al.* 1989 *Electr. Lett.* **25** 670
[60] Zhao L, Hong Q, Wang X, *et al.* 2018 *Neurocomput.* **314** 207
[61] Liu Y, Xu W J, Ma J, *et al.* 2020 *Front. Inform. Technol. Electron. Eng.*
[62] Xu Y, Ma J, Zhan X, *et al.* 2019 *Cogn. Neurodyn.* **13** 601
[63] Peixoto H M, Cruz R M, Moulin T C, *et al.* 2020 *Front. Computat. Neurosci.* **14** 5
[64] Zhao Y and Boulant J A 2005 *J. Physiol.* **564** 245
[65] Bolton C F, Sawa G M, Carter K, *et al.* 1981 *J. Neurol. Neurosur. Psych.* **44** 407
[66] Fitzhugh R 1961 *Biophys. J.* **1** 445
[67] Kyprianidis I M, Papachristou V, Stouboulos I N, *et al.* 2012 *WSEAS Tran. Syst.* **11** 516
[68] Du L, Lei Y M and Deng Z C 2019 *Sci. Chin. Technol. Sci.* **62** 1141
[69] Xiao W W, Gu H G and Liu M R 2016 *Sci. Chin. Technol. Sci.* **59** 1943
[70] Pikovsky A S and Kurths J 1997 *Phys. Rev. Lett.* **78** 775
[71] Perc M 2007 *Chaos Solitons & Fractals.* **31** 64
[72] Perc M 2005 *Phys. Rev. E* **72** 016207
[73] Sun X J, Perc M, Lu Q S, *et al.* 2008 *Chaos* **18** 023102
[74] Li Y, Xu Y and Kurth J 2016 *Phys. Rev. E* **94** 042222
[75] Xu Y, Wu J, Du L, *et al.* 2016 *Chaos Solitons Fractal.* **92** 91
[76] Wang Z Q, Xu Y and Yang H 2016 *Sci. Chin. Technol. Sci.* **59** 371
[77] Zhang H, Xu Y, Xu W, *et al.* 2012 *Chaos* **22** 043130
[78] Liu Q, Xu Y, Kurth J, *et al.* 2018 *App. Math. Mod.* **64** 249
[79] Valentia D, Augello G and Spagnolo B 2008 *Euro. Phys. J. B* **65** 443
[80] Njitacke Z T, Doubla I S, Kengne J, *et al.* 2020 *Chaos* **30** 023101
[81] Wouapi K M, Fotsin B H, Louodop F P, *et al.* 2020 *Cogn. Neurody.* **14** 135
[82] Sun K, Liu L, Qiu J, *et al.* 2020 *IEEE Tran. Fuzzy Syst.*
[83] Sun K, Qiu J, Karimi H R, *et al.* 2020 *IEEE Tran. Fuzzy Syst.* https://doi.org/10.1109/tfuzz.2020. 2979129
[84] Sun K, Qiu J, Karimi H R, *et al.* 2020 *IEEE Tran. Syst. Man. Cyber.*
[85] Wang C and Ma J 2018 *Int. J. Mod. Phys. B* **32** 1830003
[86] Wang C, Tang J and Ma J 2019 *Euro. Phys. J. Spec. Top.* **228** 1907
[87] Hodgkin A L and Huxley A F 1952 *J. Physiol.* **116** 497
[88] Hyun N G, Hyun K H, Hyun K B, *et al.* 2011 *Korean J. Physiol. Pharmacol.* **15** 371
[89] Guo D D and Lü Z S 2019 *Chin. Phys. B* **28** 110501
[90] Qu L H, Du L and Deng Z C 2018 *Chin. Phys. B* **27** 118707
[91] Yuan Z, Feng P, Du M, *et al.* 2020 *Chin. Phys. B* **29** 030504